Vertical heat flux and lateral mass transport in nonlinear internal waves

E. L. Shroyer,[1,2] J. N. Moum,[1] and J. D. Nash[1]

Received 29 January 2010; revised 4 March 2010; accepted 25 March 2010; published 24 April 2010.

[1] Comprehensive observations of velocity, density, and turbulent dissipation permit quantification of the nonlinear internal wave (NLIW) contribution to vertical heat flux and lateral mass transport over New Jersey's shelf. The effect of NLIWs on the shelf heat budget was significant. On average, heat flux in NLIWs was 10 times larger than background at the pycnocline depth. NLIWs were present at midshelf <10% of the time, yet we estimate that they contributed roughly one−half the heat flux across the pycnocline during the observation period, which was characterized by weak to moderate winds. Lateral transport distances due to the leading 3 waves in NLIW packets were typically $\mathcal{O}$(100 m) but ranged several kilometers. The month-averaged daily onshore transport (per unit alongshelf dimension) by NLIWs is estimated as 0.3 m^2s^{-1}. This is comparable to a weak downwelling wind, but sustained over an entire month. **Citation:** Shroyer, E. L., J. N. Moum, and J. D. Nash (2010), Vertical heat flux and lateral mass transport in nonlinear internal waves, *Geophys. Res. Lett.*, *37*, L08601, doi:10.1029/2010GL042715.

1. Introduction

[2] Nonlinear internal waves (NLIWs) are frequently observed in the coastal ocean [e.g., *Jackson*, 2004]. Strong shear generated by NLIWs creates conditions favorable for instabilities, producing elevated turbulent dissipation and mixing [e.g., *Sandstrom and Oakey*, 1994; *Inall et al.*, 2000; *MacKinnon and Gregg*, 2003; *Moum et al.*, 2003]. Since this mixing is often concentrated at the pycnocline, NLIWs may be a fundamental contributor to vertical nutrient and heat flux over the shelf.

[3] By definition, particle speeds (u_w) in NLIWs are comparable to the wave speed (c). Therefore, horizontal advection is important, and NLIWs transport mass as well as energy. As u_w approaches c, lateral transport distance increases; in the limit that $u_w \rightarrow c$, trapped cores of recirculating fluid form [*Lamb*, 1997]. Accordingly, NLIWs may provide an important avenue for lateral movement of fluid, larvae, and other biota.

[4] The objective here is to better quantify the NLIW contribution to these processes using data collected during the Office of Naval Research's Shallow Water experiment (SW06) on the New Jersey shelf in August 2006. Here we show that the redistribution of heat by NLIW-induced mixing was a dominant term in the vertical heat balance, during the observation period, and that NLIWs transported fluid onshore at a rate equivalent to that from weak but sustained Ekman transport.

2. Experiment and Observations

[5] NLIWs were tracked across New Jersey's shelf, using shipboard acoustics (120 kHz echosounder, 300 and 1200 kHz Doppler Current Profiler (ADCP)), X-band radar, and microstructure profiling (Figure 1, upper inset). During profiling periods, the ship was held relatively stationary as the first few waves (typically three) propagated past. Afterward, the ship re-positioned ahead of the packet and profiling resumed; this process was repeated as many as 15 times as packets evolved.

[6] Twenty-five, ship-tracked packets were used in this analysis; for reference, packets were named. Background profiles, made prior to packet arrivals, were combined with a 12-hour profiling series, to separate NLIW and background contributions to the turbulent vertical heat flux, J_q. Shipboard data were also used to compute lateral transports. This calculation was possible due to 1) high resolution of near-surface velocities (within 3–4 m) provided by the shipboard setup and 2) the ability to calculate wave speeds accurately through differencing arrival times over large distances across the shelf.

3. Vertical Heat Flux (J_q)

[7] J_q was estimated from measured dissipation (ε) and stratification (N^2) by first computing the turbulent eddy diffusivity,

$$K_\rho = \frac{\Gamma \epsilon}{N^2}, \tag{1}$$

where $\Gamma = 0.2$, is the assumed mixing efficiency [*Osborn*, 1980]. J_q was calculated as

$$J_q = \overline{\rho} C_p K_\rho T_z, \tag{2}$$

using the measured vertical temperature gradient (T_z), average density ($\overline{\rho}$), and heat capacity (C_p). Downward J_q is positive. Values above 10-m depth, where ε is contaminated by the ship's wake, were discarded. Also excluded are values where $N^2 < 5 \times 10^{-4}$ s^2, as these may produce unreasonably large K_ρ in well-mixed regions; this criterion has little influence on J_q over the extent plotted in Figure 2, and almost no effect across the pycnocline.

[8] Elevated dissipation rates were typically observed in the leading waves of each group. Often turbulent regions were confined to the trailing edge of wave interfaces, as illustrated by *Wave Mika* (Figure 1a), where increased backscatter, ε,

[1]College of Oceanic and Atmospheric Sciences, Oregon State University, Corvallis, Oregon, USA.
[2]Now at Physical Oceanography Department, Woods Hole Oceanographic Institution, Woods Hole, Massachusetts, USA

0094-8276/10/2010GL042715

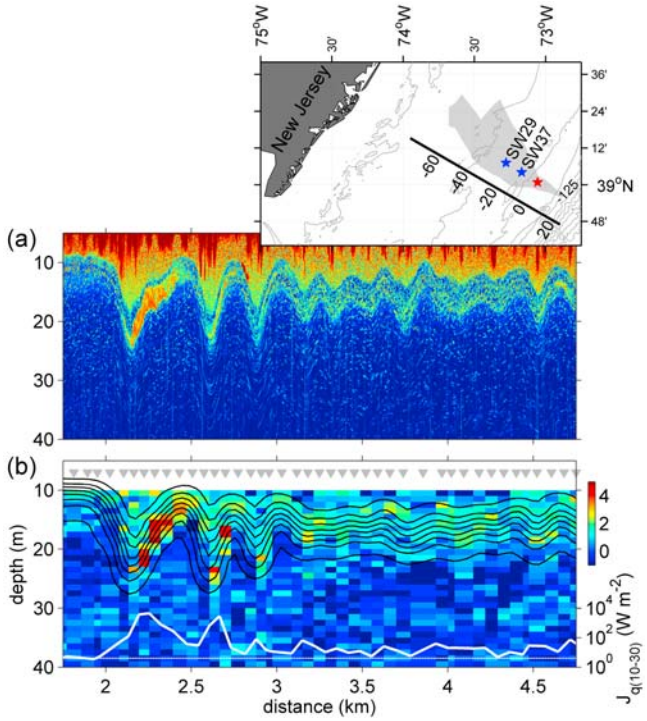

Figure 1. (a) Acoustic backscatter from 120 kHz echosounder through Mika and (b) J_q with contoured isopycnals, [21.5:23.5] kg m^{-3}. $J_{q_{(10-30)}}$ is plotted on lower right axes. Triangles mark profile positions. Transect location (red star), mooring locations (blue stars), and coordinate axis are shown in map inset. The origin is set at the position of mooring SW30, not used here. Grey cloud encompasses ship profiling positions. Inshore/offshore of the shelfbreak (125-m isobath) isobaths are plotted every 25/250 m.

and J_q were observed in the lee of the first wave trough (Figure 1b). For *Wave Mika*, J_q averaged between 10–30 m ($J_{q(10-30)}$) was 1000 times greater in the leading wave than in profiles prior to wave arrival (Figure 1b, lower right axis). Subsequent waves and the bore-like tail also exhibited elevated J_q; averaged through the extended wave train, $J_{q(10-30)}$ was 100 times greater than background levels.

3.1. Mean Vertical Profile of J_q

[9] To estimate the NLIW contribution to heat flux on the shelf, average profiles of J_q in waves, designated J_q^w, and background profiles (see section 2), designated J_q^b, were calculated (Figure 2a). The 90% bootstrapped confidence limits are shown. Fluxes were averaged in isopycnal coordinates to account for wave perturbations, and then re-mapped to depth using a mean $\rho(z)$. The average air-sea heat flux, J_q^0, was downward and estimated as 120 W m^{-2} using bulk formulae [*Fairall et al.*, 1996].

[10] Across the pycnocline, J_q^w = 790 W m^{-2} compared to J_q^b = 80 W m^{-2}. While on average, K_ρ was only 3× larger during wave passage (Figure 3), the factor-of-ten increase in J_q^w at the pycnocline results because both K_ρ and T_z are largest here. (Note that T_z was also enhanced by ~10–20% in waves.) Median values of K_ρ^b and K_ρ^w are similar, and the larger mean K_ρ^w is due to the infrequent occurrence of extremely large values. In other words, short episodes of wave activity were highly effective in redistributing heat below the thermocline.

3.2. Time-weighted Average of J_q

[11] The fraction of time (P^w) NLIWs were present at a specific location was estimated by using the squared vertical velocity (w^2) from upward-looking 300 kHz ADCPs moored on moorings SW37 and SW29 (Figure 1) as a NLIW metric. Data were filtered to include signals with periods between 2 and 10 minutes. A cut-off of $w_c^2 = 4 \times 10^{-4}$ m^{2}s^{-2} was established using the median value of the depth-maximum of w^2 in ship-tracked waves. This method estimates that $P^w = 0.053$ at SW29 and $P^w = 0.085$ at SW37 (with an average $P^w = 0.07$). Although these estimates are sensitive to w_c^2 (a factor of 2 change in w_c^2 alters P^w by a factor of 2–2.5), $w_c^2 = 4 \times 10^{-4}$ms^{-2} is directly based on shipboard observations from which J_q^b and J_q^w were created. Since we use the ship-measured median to establish w_c^2, we believe that $P^w = 0.07$ is conservative; this assessment agrees with a qualitative

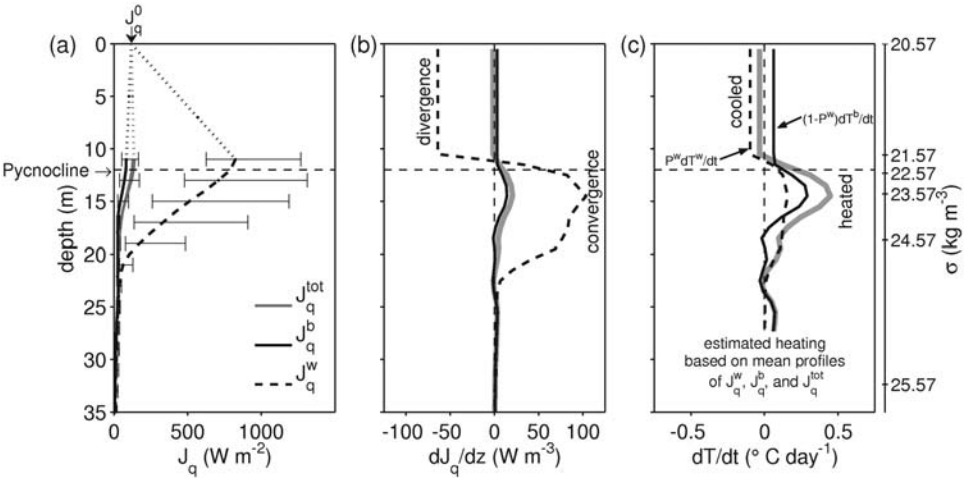

Figure 2. (a) J_q, (b) dJ_q/dz, and (c) dT/dt for the background (black), waves (dashed), and time-weighted total (grey). Profiles were filtered to exclude scales smaller than 7 m, and the 90% bootstrapped confidence interval is plotted for J_q^b and J_q^w. Arrow at top show average air-sea heat flux. dJ_q/dz and dT/dt are based on mean profiles of J_q, which were extrapolated upwards linearly to J_q^0 before differencing (dotted lines, panel a).

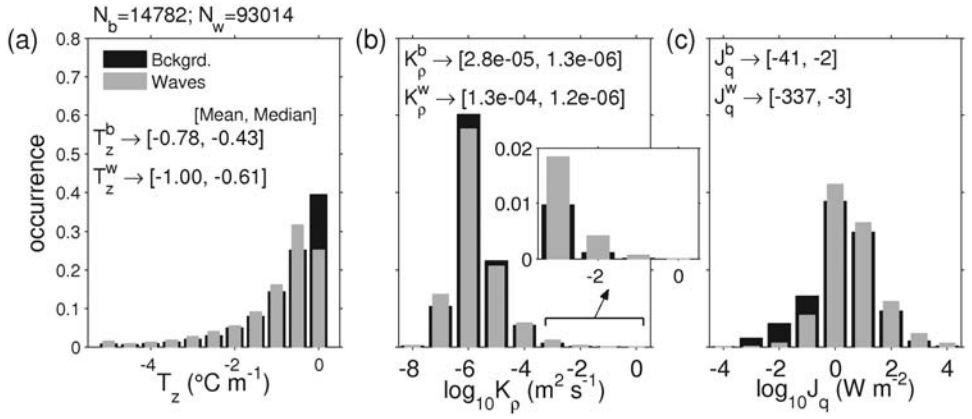

Figure 3. Histograms of (a) T_z, (b) $K\rho$, and (c) J_q for background and wave conditions. Mean and median values are given. The number of samples, N_w and N_b, used to compose histograms tally the 1-m bins averaged into J_q^w and J_q^b (Figure 2a).

evaluation of time series at SW29, which estimated $P^w = 0.10$. A supplement is available detailing the use of w_c^2 in selecting times of NLIWs.

[12] The NLIW contribution to the net cross-pycnocline heat flux is

$$\%\ \text{Heat Flux by Waves} = \frac{P^w J_q^w}{P^w J_q^w + (1 - P^w) J_q^b} \times 100, \qquad (3)$$

where $P^w = 0.07$. Based on 90% error limits of J_q, NLIWs contributed between 20–67% of the heat flux across the pycnocline. (At the pycnocline, error bounds are [577, 1304] W m^{-2} for J_q^w and [48, 172] W m^{-2} for J_q^b.) Using mean profiles, the time-weighted total heat flux ($J_q^{tot} = P^w J_q^w + (1 - P^w) J_q^b = 130$ W m^{-2}) at the pycnocline is close to J_q^0.

[13] The divergence of the heat flux (Figure 2b) is expressed through the one-dimensional balance,

$$\frac{dT}{dt} = -(\overline{\rho} C_p)^{-1} \frac{dJ_q}{dz}, \qquad (4)$$

plotted in Figure 2c. Here, J_q^w and J_q^b were extended linearly to J_q^0 at $z = 0$ before applying equation 4. Note dT/dt is an estimate based on mean profiles of J_q, but uncertainty in J_q and Γ, which can influence the relationship between J_q and J_q^0, can change the shape of dJ_q/dz. However, within reasonable error bounds, mixing associated with NLIWs resulted in a divergence of J_q in the surface layer. Using mean profiles, we estimate that during wave passage the mixed layer cooled at the rate of 1°C per day (calculated by averaging the wave contribution, dT^w/dt, from the surface to the pycnocline depth), yielding an average rate of $P^w dT^w/dt \sim 0.1$°C per day. Net heating in the background state, $(1-P^w)$ $dT^b/dt \sim 0.1$°C per day, balanced cooling by NLIWs, so that the total dT/dt (or equivalently dJ_q/dz) was near zero in the surface layer. This means that J_q^0 was transported without modification through the pycnocline by the contributions from wave and background divergences. dT/dt is negligible below 25-m depth; this is likely associated with reduced T_z and exclusion of the bottom boundary layer in our measurements. dT/dt only reflects heating/cooling due to vertical processes; lateral advection may independently heat/cool the mixed layer.

[14] Our assessment of the relative contribution from NLIWs depends on the background mixing, which, during SW06, was driven by mild winds (mean speeds were 6 m/s, and speeds >12 m/s occurred only 3% of the time). The response of the shelf to a large storm would change this result considerably as a consequence of increased wind-driven mixing and possibly a weaker NLIW field associated with reduced stratification. Depending on the pycnocline depth our estimates of J_q^b may be biased toward values in the lower pycnocline, although the average maximum stratification was located beneath 10-m depth as indicated in Figure 2.

4. Particle Transport Distance

[15] Particle transport distance, Δ, was calculated as

$$\Delta = \int_{x_R'}^{x_L'} \frac{u_w(x')}{c - u_w(x')} dx', \qquad (5)$$

following *Lamb* [1997]. The wave particle velocity, u_w, is a function of the spatial coordinate in the wave's reference frame, $x' = x - ct$, and depends upon the wave speed, c. Velocity was extrapolated to the surface assuming a constant horizontal velocity above the uppermost ADCP bin, and u_w was calculated by subtracting the background velocity interpolated along streamlines. With the assumption that streamlines follow isopycnals, equation 5 was evaluated along constant density surfaces to find Δ as a function of undisturbed depth (Figure 4a). Note in the limit $u_w \to c$, $\Delta \to \infty$, corresponding to the case of a trapped core. While our observations do not show trapped cores, Δ becomes large as u_w approaches c.

[16] Based on theory, u_w and Δ should be maximum at the surface (e.g., *Rosey*, Figure 4a); however, sometimes the observed maximum u_w was beneath the surface (e.g., *Kevin* and *Mika*). A possible cause could be the failure to account for a near-surface offshore background current, which would not be resolved by ship measurements. In such cases, the calculated surface transport, denoted as Δ^s, is likely an underestimate of its true value. Regardless, Δ^s is used below to assess NLIW transport distances.

4.1. Average Δ^s for Ship-Tracked Waves

[17] The surface transport, Δ^s, was calculated for the leading three waves in each group, by evaluating equation 5 at $z = 0$ and integrating across the first three waves. On average,

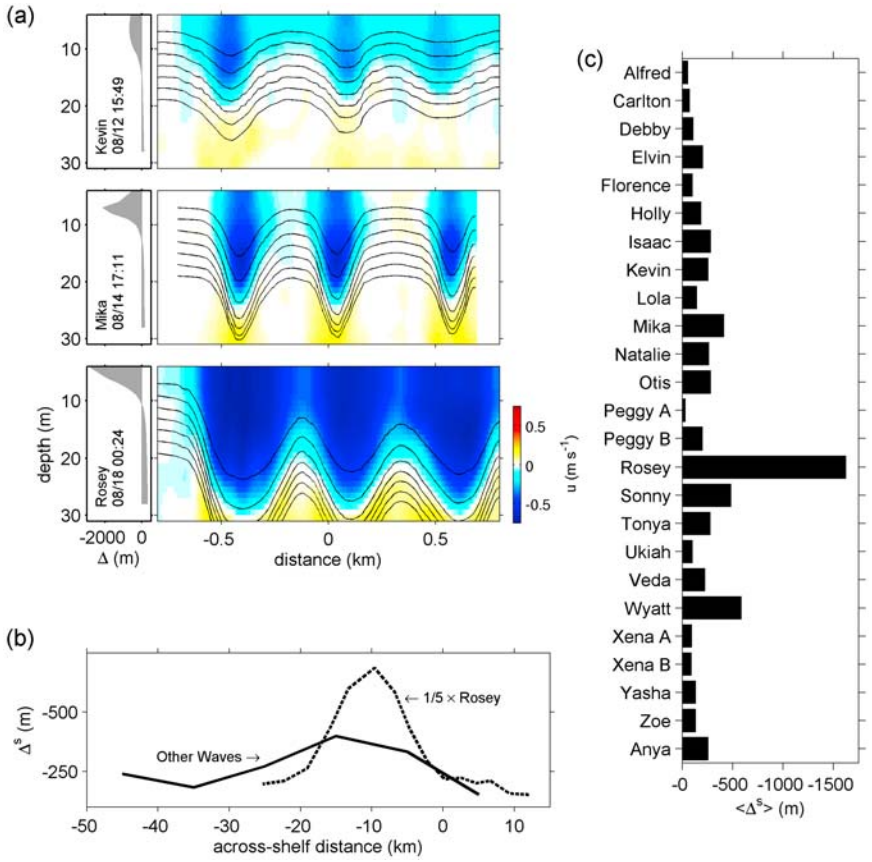

Figure 4. (a) Left panels show Δ as a function of initial particle depth for the leading three waves. Negative transports are shoreward. Right panels show u_w for three packets: *Kevin* at −15.25 km, *Mika* at −27.5 km, and *Rosey* at −7.25 km. Shipboard 300 and 1200 kHz ADCPs were meshed to produce u_w. Isopycnals originating at z = (7, 9, 11,…, 19) m are contoured. (b) The ten-kilometer bin averaged Δ^s excluding *Rosey* (solid line) and one-fifth of *Rosey*'s Δ^s (dashed line). (c) Shelf-averaged $\langle\Delta^s\rangle$ of the three leading waves for each packet.

$\Delta^s \approx -200$ m. The ten-kilometer bin-averaged Δ^s varied across the shelf, with a peak at $x = -15$ km of $\Delta^s \approx -400$ m (Figure 4b, solid line). At this location, waves typically reached maximum amplitude. The bin-average excludes *Rosey*, which produced much larger Δ^s (Figure 4b, dashed line). *Rosey* had the largest observed amplitude (in excess of 20 m) and was highly nonlinear. The character difference between *Rosey* and other waves is evident in Figure 4a.

[18] Shelf-averaged transports ($\langle\Delta^s\rangle$) of individual packets are shown in Figure 4c. Averages were made over a variety of time ($\mathcal{O}$(1 hr to 1 day)) and spatial ($\mathcal{O}$(1–50 km)) scales depending on how long packets were tracked. For most waves, $\langle\Delta^s\rangle$ was a few hundred meters. In larger-amplitude packets, e.g., Sonny and Wyatt, $\langle\Delta^s\rangle$ was ~500 m, and near $x = -15$ km, Δ_s exceeded 1 km. For *Rosey*, Δ^s exceeded 2 km at multiple locations, and $\langle\Delta^s\rangle$ was ~1.5 km.

4.2. Extrapolation to All NLIWs

[19] Δ_s represents transport by the first three waves, but packets were typically comprised of over ten waves on the shelf. For example, *Mika*/*Rosey* consisted of 13/16 waves at mooring SW30 ($x = 0$ km); these numbers increased to 20/30 at SW29, located 20 km further inshore. Average surface transports can be approximated as 1–2 km, after extension to the entire packet. However, for *Rosey*, transports were likely near 10 km in the mid-shelf region. Although *Rosey* was anomalous in the ship-based record, one other packet of a similar size was documented in the mooring record.

[20] Ship-tracked waves accounted for less than one-third of the waves observed at moorings. Over some time periods multiple packets (as many as four) were observed per M2 tidal period. These considerations suggest that the average daily transport distance associated with NLIWs would be several kilometers, even neglecting *Rosey*. Thus, under certain conditions, moderate NLIWs are capable of transporting mass $\mathcal{O}$(10 km) shoreward, particularly near $x = -15$ km. Occasionally, when a very large amplitude wave is formed, a similar transport distance may be achieved by just one packet.

[21] This analysis is sensitive to estimated c and ignores contributions due to a particle's relative horizontal speed (i.e., swimming fish). As a test on sensitivity associated with these considerations, the above calculation was repeated using a constant swimming speed of 0.1 m s^{-1}, which is equivalent to reducing c by 0.1 m s^{-1}. The result increased Δ^s by 100 m for most waves, but more than doubled that of *Rosey*.

5. Discussion and Summary

[22] To quantify the effects of NLIWs to the shelf environment, NLIW-driven heat fluxes and lateral transport distances were calculated using observations from the New

Jersey shelf. Heat flux in the waves was approximately ten times larger than the background heat flux across the pycnocline, and NLIWs contributed between 20–65% of the total heat flux in a time-weighted sense. The enhancement of heat flux by waves was primarily attributed to larger values of turbulent diffusivity that occurred near the pycnocline. The result can be extended to nutrients and other tracers whose distributions are aligned with the pycnocline.

[23] Our estimates of J_q^w are similar to those made by *Moum et al.* [2003] off Oregon who measured fluxes greater than 2000 W m^{-2} in NLIWs. In contrast, *Inall et al.* [2000] estimated across-pycnocline fluxes as 80 W m^{-2} on the Malin shelf for a 12.42-hour period marked by NLIWs; the smaller number may be attributed to a combination of factors, including differences in NLIW fields and sampling schemes. Not surprisingly, estimates of J_q presented here are dwarfed by those acquired during the passage of a tropical storm in the Mid-Atlantic, in which $J_q \gtrsim 10^4$ W m^{-2} was sustained over most of a day (P. Wiles et al., Glider measurements of cross-pycnocline heat flux during the passage of Tropical Storm Hanna over the Mid-Atlantic Bight, manuscript in preparation, 2010).

[24] Lateral transport distances were in most cases roughly 1–2 kilometers per packet; however, one packet (*Rosey*) was capable of transporting mass ~10 km. So that these estimates may be compared to other mechanisms of cross-shelf exchange [*Huthnance*, 1995], transport distances are converted to vertically-integrated transports (units of m^{2}s^{-1}) using $\overline{U} = \int \Delta(z)/\tau(z) dz$, evaluated from the surface down to the first zero-crossing of $\Delta(z)$. Here, $\tau(z)$ is the amount of time a parcel of water at a given rest depth was advected by the wave. On average, $\overline{U}$ was −4.6 m^{2}s^{-1}; and, the maximum $\overline{U}$ was −21.2 m^{2}s^{-1}. Since NLIWs were present roughly 7% of the time, the month-long average daily NLIW transport is estimated as −0.3 m^{2}s^{-1}. The daily average and maximum transport are similar to those estimated by *Inall et al.* [2001] on the Malin shelf. The maximum is much greater than those estimated by *Huthnance* [1995] (Table 1), but the mean is of the same magnitude.

[25] NLIW transport varied both across the shelf, since waves reached maximum transports 40 km inshore of the shelf break, and in time, since larger waves were observed from the 17–22 August. For example, the average transport of wave groups– *Rosey*, *Sonny*, and *Tonya*– is −9.4 m^{2}s^{-1}, corresponding to an average daily transport of −0.7 m^2 s^{-1}. This value is comparable to the onshore transport of a sustained downwelling wind stress of 0.07 N m^{-2}.

[26] Our estimates indicate that NLIWs are significant contributors to two important aspects of shelf dynamics, at least under conditions of weak to moderate atmospheric forcing. In summer, and during weak surface forcing, we expect the surface layer to heat considerably in the absence of NLIWs or compensatory lateral advection. Here, we estimated that NLIWs acted to maintain the surface mixed layer in near-steady state, transporting heat input at the surface through the pycnocline. The onshore mass transport due to NLIWs is comparable to that due to a weak, but sustained (over the course of a month) downwelling breeze.

[27] **Acknowledgments.** This work was funded by the Office of Naval Research. We thank the Captains and crews of the *R/V Oceanus* and the *R/V Knorr*, along with Greg Avicola, James Irish, Sam Kelly, John Kemp, Ray Kreth, James Lynch, Mike Neeley-Brown, and Alexander Perlin who helped with ship- and mooring-operations.

References

Fairall, C. W., E. F. Bradley, D. P. Rogers, J. B. Edson, and G. S. Young (1996), Bulk parameterization of air-sea fluxes for Tropical Ocean-Global Atmosphere Coupled-Ocean Atmosphere Response Experiment, *J. Geophys. Res.*, *101*, 3747–3764, doi:10.1029/95JC03205.

Huthnance, J. M. (1995), Circulation, exchange and water masses at the ocean margin: The role of physical processes at the shelf edge, *Prog. Oceanogr.*, *35*, 353–431.

Inall, M. E., T. P. Rippeth, and T. J. Sherwin (2000), Impact of nonlinear waves on the dissipation of the internal tidal energy at a shelf break, *J. Geophys. Res.*, *105*(C4), 8687–8705.

Inall, M., G. Shapiro, and T. Sherwin (2001), Mass transport by non-linear internal waves on the Malin Shelf, *Cont. Shelf Res.*, *21*, 1449–1472.

Jackson, C. R. (2004), *An Atlas of Internal Solitary-like Waves and their Properties* [electronic], 2nd ed., Global Ocean Assoc., Alexandria, Va. (Available at www.internalwaveatlas.com).

Lamb, K. G. (1997), Particle transport by nonbreaking internal solitary waves, *J. Geophys. Res.*, *102*, 18,641–18,660.

MacKinnon, J. A., and M. C. Gregg (2003), Mixing on the late-summer New England shelf—Solibores, shear and stratification, *J. Phys. Oceanogr.*, *33*, 1476–1492.

Moum, J. N., D. M. Farmer, W. D. Smyth, L. Armi, and S. Vagle (2003), Structure and generation of turbulence at interfaces strained by internal solitary waves propagating shoreward over the continental shelf, *J. Phys. Oceanogr.*, *33*, 2093–2112.

Osborn, T. R. (1980), Estimates of the local rate of vertical diffusion from dissipation measurements, *J. Phys. Oceanogr.*, *10*, 83–89.

Sandstrom, H., and N. S. Oakey (1994), Dissipation of internal tides and solitary waves, *J. Phys. Oceanogr.*, *25*, 604–614.

J. N. Moum and J. D. Nash, College of Oceanic and Atmospheric Sciences, Oregon State University, 104 Ocean Admin. Bldg, Corvallis, OR 97331-5503, USA.

E. L. Shroyer, Physical Oceanography Department, Woods Hole Oceanographic Institution, Clark 316A, MS21, Woods Hole, MA 02543, USA. (eshroyer@whoi.edu)